Journal of Electronics, Electromedical Engineering, and Medical Informatics
Homepage: jeeemi.org; Vol. 8, No. 2, April 2026, pp: 825-842 e-ISSN: 2656-8632

RESEARCH ARTICLE OPEN ACCESS

Deep Electro-Impedance Analytics for Bone Mineral Profiling: A Rough-Fuzzy Neural Attention Model

Aripin, Mauldy Nawa Ayu Wulandari, Eunike Laurensya Agata, Zulhendra Adi Kusuma, Susilo, and Sari Ayu Wulandari

Faculty of Engineering, Universitas Dian Nuswantoro, Semarang, Indonesia

Corresponding author: Sari Ayu Wulandari (e-mail: sari.wulandari@dsn.dinus.ac.id), **Author(s) Email**: Aripin (e-mail: arifin@dsn.dinus.ac.id), Mauldy Nawa Ayu Wulandari (e-mail: 513202200241@mhs.dinus.ac.id) Eunike Laurensya Agata (e-mail: 513202200233@mhs.dinus.ac.id), Zulhendra Adi Kusuma (e-mail: 513202200208@mhs.dinus.ac.id), Susilo (e-mail: susilosumarto@gmail.com)

Abstract **Electrochemical Impedance Spectroscopy (EIS) has emerged as a promising modality for non-invasive biomedical diagnostics, particularly for radiation-free monitoring tasks such as Bone Mineral Density (BMD) assessment. However, the high dimensionality, noise, and non-linear behavior of impedance signals pose significant challenges for accurate and interpretable prediction. This study introduces Hybrid Rough Set-Attention Network (HRSA-Net), a hybrid regression framework that combines Rough Set-based feature selection with a self-attention neural architecture to enable continuous BMD estimation directly from raw EIS data. The proposed framework employs Artificial Neural Network (ANN) and Transformer-based regression models to learn complex impedance-density relationships. Unlike prior studies that are limited to classification tasks or rely on indirect physiological indicators, HRSA-Net is explicitly designed for direct regression of real-valued BMD scores. The model performance is evaluated against reference measurements obtained from Dual-energy X-ray Absorptiometry (DXA), the current clinical gold standard for bone density assessment. Through a comprehensive series of ablation experiments, HRSA-Net achieves an R^2 of 0.834 using an attention-guided ANN backbone, demonstrating the critical contribution of both Rough Set reduction and attention mechanisms. Performance further improves to an R^2 of 0.855 when incorporating a Transformer regressor and Huber loss, indicating superior robustness and generalizability under varying signal conditions. Comparative analysis with state-of-the-art EIS-based learning approaches shows that the proposed pipeline consistently outperforms conventional neural models and statistical methods. Overall, HRSA-Net provides an interpretable, accurate, and scalable foundation for future portable EIS-based BMD diagnostic systems, offering a safer alternative to radiological methods such as DXA and enabling feasible deployment in primary or community healthcare settings.**

Keywords **Electrochemical Impedance Spectroscopy; Bone Mineral Density; Non-invasive diagnostics; Deep regression**.

I. Introduction

According to the World Health Organization (WHO), osteoporosis affects more than 200 million people globally and contributes to over 8.9 million fractures each year [1]. Bone Mineral Density (BMD) is a critical marker used to assess bone strength and diagnose osteoporosis and related conditions [2]. Dual-energy X-ray Absorptiometry (DXA) has become the clinical gold standard for BMD measurement due to its precision and reproducibility [3]. However, despite its effectiveness, DXA involves exposure to ionizing radiation, requires expensive and non-portable equipment, and is not always accessible for routine or community-based screening [4]. Moreover, DXA lacks real-time monitoring capabilities and cannot be safely used in certain populations such as children and pregnant women [5]. These limitations necessitate the development of non-radiative, safe, and cost-effective alternatives for bone density assessment. Several studies have demonstrated that electrical bioimpedance and Electrochemical Impedance Spectroscopy (EIS) measurements exhibit significant correlation with Bone Mineral Density (BMD) values obtained using Dual-energy X-ray Absorptiometry

Manuscript received 26 Dec 2025; Revised 10 Feb 2026; Accepted 20 April 2026; Available online 30 April 2026
Digital Object Identifier (**DOI**): https://doi.org/10.35882/jeeemi.v8i2.1434

(DXA). Variations in bone mineralization and porosity influence the electrical conductivity and impedance characteristics of bone tissue, enabling impedance-based techniques to indirectly reflect mineral density changes. In recent years, Electrochemical Impedance Spectroscopy (EIS) has gained attention as a promising technique for probing the electrical properties of biological tissues [6]. EIS measures frequency-dependent impedance, which can reflect structural and compositional changes in tissue, including variations in bone porosity and mineralization [7]. As a non-invasive and radiation-free method, EIS is highly suitable for frequent monitoring and has demonstrated potential in early-stage diagnostics and tissue health assessment [8][9]. Previous investigations reported that impedance-derived parameters can distinguish between normal, osteopenic, and osteoporotic bone conditions with clinically meaningful agreement when compared to DXA measurements [7][8][10][11].

Although EIS does not directly measure mineral attenuation as performed in radiological imaging, its sensitivity to structural and compositional tissue properties allows it to serve as a promising radiation-free alternative for preliminary screening and longitudinal monitoring of bone health. Consequently, EIS-based predictive modeling has gained increasing attention as a feasible complementary approach to DXA, particularly for portable, low-cost, and community-level osteoporosis assessment. Recent advances in machine learning have further expanded the potential of EIS-based diagnostic systems. Data-driven approaches such as Artificial Neural Networks (ANN), Support Vector Machines (SVM), and ensemble learning techniques have been widely applied to model the complex nonlinear relationship between impedance features and physiological parameters [12][13]. However, many existing approaches focus on classification tasks rather than continuous regression, limiting their applicability for precise bone mineral density estimation [14].

In biomedical applications, model interpretability is increasingly recognized as a critical requirement alongside predictive accuracy. Techniques such as Rough Set theory provide a principled framework for feature dependency analysis and rule-based interpretation, which are particularly valuable in medical decision support systems [15][16]. Integrating interpretable feature selection with deep learning architectures offers a pathway toward accurate yet explainable regression models for clinical use [17].

Table 1. Summary of existing EIS-Based studies and the contributions of this work.

Ref.	Research Focus	Limitation	Contribution of This Study
[33]	EIS with deep learning for moisture estimation	Not generalized to biological tissue density	Extended impedance-based learning to non-invasive BMD regression
[34]	LSTM-based soil nitrate prediction using EIS	Not biomedical-oriented; focuses on chemistry	Introduced fuzzy rough set preprocessing to handle high-variance EIS signals
[42]	Review of EIS in disease diagnosis	Lacks a specific bone predictive	Applied a hybrid CNN-BiLSTM–Attention learning model for BMD
[47]	Potential of EIS for healthy vs. osteopenic bone	Manual feature analysis without automated DL	Automated feature extraction using deep learning for continuous BMD value estimation
[48]	Skin cancer detection EIS	Limited to binary classification tasks	Developed a high-resolution regression framework for quantitative BMD
[50]	Blood glucose detection	Not integrated with ML frameworks	Enhanced model interpretability and accuracy using Attention
[51]	Diabetes classification using EIS + BP	Basic ML, lacks temporal sequence	Utilized BiLSTM to capture complex frequency in EIS
[52]	Scaffold degradation via EIS	Focuses on material degradation	Enabled real-time BMD monitoring
[18]	DL for oral disorder detection via EIS	Limited to sequence analysis	Hybrid model generalization for large-scale, multi-frequency EIS
[53]	ML-directed EIT for plaque prediction	Focused on vascular health rather than skeletal mineralogy	Adapted impedance tomography principles for skeletal health monitoring via spectral regression

Manuscript received 26 Dec 2025; Revised 10 Feb 2026; Accepted 20 April 2026; Available online 30 April 2026
Digital Object Identifier (**DOI**): https://doi.org/10.35882/jeeemi.v8i2.1434

To further enhance EIS-based bone evaluation, machine learning techniques, particularly deep learning, have been integrated to model the complex relationships between impedance patterns and physiological parameters [18]. Among them, neural network-based regression and feature extraction techniques offer a pathway toward calibration-free and portable BMD monitoring systems. However, high-dimensional impedance data is often noisy, redundant, and highly non-linear, posing challenges in robust modeling [15].

Recent biomedical signal research has highlighted the effectiveness of advanced deep learning models in medical data interpretation, including transformer-based architectures for disease detection and fuzzy logic-based signal enhancement approaches [18][19][20][21]. These studies demonstrate the growing importance of combining signal processing techniques with learning-based interpretation to improve robustness in biomedical diagnostics. However, existing EIS-based Bone Mineral Density (BMD) estimation approaches often rely on black-box deep learning models that suffer from high-dimensional noise, limited interpretability, and poor generalization under low-signal conditions [18][22]. Recent biomedical AI studies have shown that non-invasive diagnostic systems can benefit from deep learning-based feature extraction and predictive modeling, particularly for screening applications where portability and accessibility are important [23][24][25]. Recent advances in biomedical signal analysis have emphasized the importance of integrating interpretable feature selection mechanisms with deep neural architectures to simultaneously improve prediction accuracy and model transparency. Rule-based feature selection approaches, such as Rough Set Theory (RST), have been widely utilized to identify dependency-driven attributes and eliminate redundant information in high-dimensional biomedical datasets without requiring probabilistic assumptions [15][26][27], thereby enhancing interpretability while reducing computational complexity. In parallel, attention-driven neural architectures, including self-attention networks and Transformer models, have demonstrated superior capability in capturing contextual relationships and long-range feature dependencies in physiological signal modeling and medical regression tasks [28][29][30].

Despite these advances, most existing studies apply feature selection and attention-based learning independently. The integration of rule-based dependency reduction with attention-guided regression remains relatively underexplored, particularly in Electrochemical Impedance Spectroscopy (EIS)-based bone density estimation [18][31][32]. To address this limitation, this study proposes a non-radiative, interpretable, and accurate framework for predicting BMD directly from EIS signals through a Hybrid Rough Set–Attention Neural Network (HRSA-Net). The proposed framework integrates Rough Set-based feature reduction with an attention-driven neural regression architecture, enabling adaptive prioritization of impedance features while preserving model interpretability. This hybrid design reduces dimensional redundancy, improves robustness against noisy measurements, and enables continuous estimation of clinically meaningful BMD values. A summary of related works and the contributions of this study are presented in Table 1. The main contributions of this paper are summarized as follows:

1. Integration of Rough Set Theory for Feature Selection: We apply RST to reduce dimensionality and extract dependency-based features from high-dimensional EIS signals, eliminating irrelevant or redundant inputs.
2. Attention-Based Neural Prediction Framework: We design a deep neural network incorporating attention mechanisms to prioritize feature importance and improve BMD prediction performance.
3. Non-Radiative BMD Estimation via EIS: We propose a non-invasive, radiation-free framework for estimating bone mineral content using impedance signals, offering a safer and more accessible alternative to DXA.
4. Comprehensive Evaluation and Benchmarking: We evaluate the proposed method on real EIS data and compare it against baseline neural models and state-of-the-art feature selection techniques.

As summarized in Table 1, previous EIS-based learning studies exhibit several common limitations that restrict their applicability for accurate bone mineral density estimation. First, many existing approaches focus primarily on classification problems rather than continuous regression, limiting their ability to provide quantitative BMD values required for clinical assessment. Second, several deep learning models rely on high-dimensional impedance inputs without interpretable feature reduction, which may introduce redundancy and reduce model transparency. Third, conventional neural architectures often lack mechanisms for adaptive feature weighting, resulting in reduced robustness under noisy or low-signal measurement conditions. The proposed HRSA-Net framework is designed to address these limitations through three key strategies. The integration of Rough Set Theory enables dependency-based feature reduction, eliminating irrelevant impedance attributes while preserving interpretability. Furthermore, the incorporation of attention mechanisms allows adaptive

Manuscript received 26 Dec 2025; Revised 10 Feb 2026; Accepted 20 April 2026; Available online 30 April 2026
Digital Object Identifier (**DOI**): https://doi.org/10.35882/jeeemi.v8i2.1434

prioritization of informative spectral features, improving regression stability and generalization performance. Unlike prior studies limited to categorical prediction, the proposed approach performs direct continuous regression of Bone Mineral Density values derived from reference measurements, thereby providing clinically meaningful estimation outcomes.

The remainder of this article is organized as follows. Section II describes the proposed HRSA-Net methodology and dataset preparation. Section III presents the experimental results and performance evaluation. Section IV discusses the findings and model implications. Finally, Section V concludes the paper and outlines future research directions.

II. Method

A. Dataset Description

The proposed method focuses on evaluating the performance of various loss functions using a hybrid model combining rough set theory and attention-based deep regression (see Fig. 1). We utilized the primary dataset, comprising 1000 rows of EIS data as mentioned in Table 2, where each row contains impedance features across columns A–CW (totaling more than 90 features).

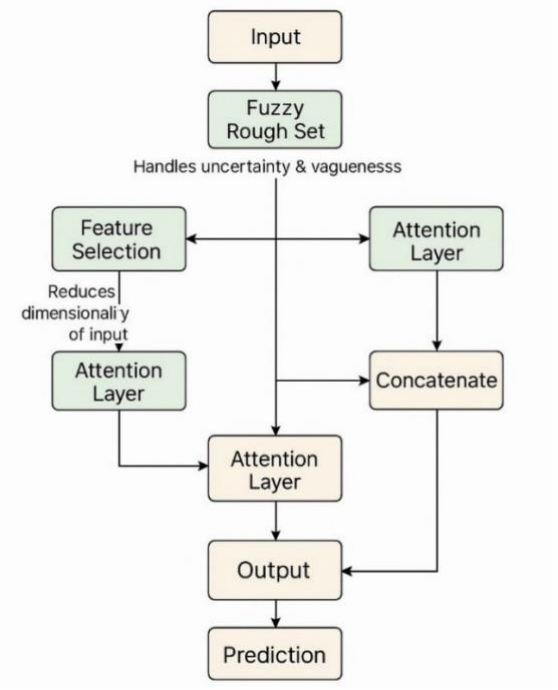

Fig. 1. Architecture of the proposed Hybrid Rough Set-Attention Neural Network (HRSA-Net).

These are frequency-dependent impedance measurements extracted from a phantom bone model. Corresponding to each impedance sample is a label derived from DEXA bone mineral density classification (ground truth), categorized into 8 groups. The dataset distribution is as follows: Normal class includes 4 groups of 125 samples each (totaling 500), Osteopenia includes 3 groups of 125 samples (375 total), and Osteoporosis includes 1 group of 125 samples. The label values represent real-valued BMD scores used as regression targets (shown in Table 2).

Table 2. Detailed description of phantom-based Electrochemical Impedance Spectroscopy (EIS) dataset including Bone Mineral Density values and clinical classification used for model training.

Type Phantom	Region	BMD (g/cm²)	Class Category	Samples
1	L1	1.327	Normal	125
1	L2	1.167	Normal	125
1	L3	1.011	Osteopenia	125
1	L4	0.794	Osteopenia	125
2	L1	1.239	Normal	125
2	L2	1.053	Normal	125
2	L3	0.903	Osteopenia	125
2	L4	0.716	Osteoporosis	125

B. Model Architecture: Hybrid Rough Set-Attention Neural Network (HRSA-Net)

The proposed HRSA-Net framework aims to predict Bone Mineral Density (BMD) from raw Electrochemical Impedance Spectroscopy (EIS) data using a hybrid approach that integrates Rough Set Theory (RST) for feature reduction and an Attention-based Neural Network for regression. This method leverages the rule-based interpretability of rough sets and the dynamic focusing capability of attention layers to address the challenges of high-dimensional, noisy, and non-linear EIS signals [9][18].

Each EIS measurement produces a set of frequency-dependent impedance values, typically captured over a logarithmic frequency sweep. The raw data matrix $Z \in \mathbb{R}^{nxf}$, where the raw data matrix is represented as $Z \in \mathbb{R}^{nxf}$, where n denotes the number of samples (for example, 500 EIS spectra) and f represents the number of frequency points or features per spectrum (typically ranging from 100 to 200). The element Z(i,j) corresponds to the impedance magnitude or phase measured at the j-th frequency point for the i-th sample. This raw matrix is first normalized using min-max or z-score normalization to obtain Eq. (1) [15].

$$X = Normalize\,(Z) \in \mathbb{R}^{nxf} \quad (1)$$

Manuscript received 26 Dec 2025; Revised 10 Feb 2026; Accepted 20 April 2026; Available online 30 April 2026
Digital Object Identifier (**DOI**): https://doi.org/10.35882/jeeemi.v8i2.1434

Table 3. Representative example of feature selection before and after Rough Set–Based dependency reduction applied to EIS impedance features.

Feature Index	Frequency (kHz)	Impedance Type	Before Reduction	After Reduction
F1	1	Magnitude	Yes	Yes
F8	5	Magnitude	Yes	No
F15	10	Phase	Yes	Yes
F27	25	Magnitude	Yes	No
F42	50	Phase	Yes	Yes

Rough Set Theory is applied to reduce the dimensionality of X and identify the most discriminative features. First, the continuous matrix X is discretized using entropy-based binning as Eq. (2).

$$D_{i,j} = DiscretizeX_{i,j} \quad (2)$$

Rough Set theory has been widely applied in biomedical signal processing for feature reduction and dependency analysis, especially in high-dimensional and noisy datasets [26]. By identifying the most informative feature subsets without requiring prior probabilistic assumptions, Rough Set-based methods can enhance model robustness and reduce redundancy in impedance-derived features [27]. Attention mechanisms have demonstrated strong performance in capturing long-range dependencies and salient feature interactions in biomedical data analysis [28]. More recently, Transformer-based architectures have been adopted for regression tasks, including physiological signal modeling and medical parameter estimation, due to their ability to learn contextual representations efficiently [29][30]. These properties make attention-driven regression models particularly suitable for EIS-based bone density estimation.

Next, an indiscernibility relation is formed to group samples with identical attribute values. A dependency degree $\gamma(F, d)$ computed to evaluate the importance of each feature subset *F* with respect to decision labels *d* (BMD values) as Eq. (3).

$$\gamma(F, d) = \frac{|POS_F(d)|}{|U|} \quad (3)$$

where $POS_F(d)$ denotes the positive region, and *U* is the universe of samples. Only features with γ values above a predefined threshold are retained [31,32], resulting in a reduced feature $X_{reduced} \in \mathbb{R}^{nxf}$. This reduced matrix $f' \ll f$ is then fed into an attention-based regression network. The attention mechanism computes importance weights for each feature as described in Eq. (4).

$$\alpha_j = \frac{exp(e_j)}{\sum_{k=1}^{f'} exp(e_k)} \text{ with } e_j = \omega^T tanh(W_a x_j + b_a) \quad (4)$$

The final context vector is computed as the weighted sum in Eq. (5).

$$\sum_{i,j=1}^{f'} \alpha_j x_{ij} \quad (5)$$

This context vector c_i is then passed through fully connected layers as Eq. (6).

$$\hat{y}_i = \sigma(W_r \cdot c_i + b_r) \quad (6)$$

where $y_i \in \mathbb{R}$ is the predicted BMD value for the i-th sample, W_r is the regression weights, and σ is a linear or non-linear activation function [33,34]. The model is trained using Mean Squared Error (MSE) as the loss function, as Eq. (7).

$$L = \frac{1}{n}\sum_{i=1}^{n}(y_i - \hat{y}_i)^2 \quad (7)$$

where y_i is the true BMD value from the ground truth. Training is optimized using the Adam optimizer with an early stopping criterion based on validation loss [35].

C. Rough Set Reduction Evidence

To provide clearer insight into the Rough Set-based feature reduction process, an analysis was conducted to compare impedance features before and after dependency-based selection based on Rough Set Theory (RST) [15][26]. The original EIS dataset consists of high-dimensional frequency-dependent impedance attributes extracted across multiple measurement points. After discretization and dependency evaluation, only features contributing significantly to Bone Mineral Density (BMD) prediction were retained. Features with low dependency values were considered redundant or irrelevant and therefore eliminated from the learning process. As illustrated in Table 3, Rough Set reduction decreases the feature dimensionality from 96 original impedance attributes to 28 dependency-relevant features, corresponding to a reduction of approximately 70.8%. This substantial dimensionality reduction helps eliminate redundant and irrelevant impedance attributes while preserving the most informative features required for accurate regression modeling. By reducing the input feature space, the model becomes more efficient and less prone to overfitting when processing high-dimensional EIS signals.

Manuscript received 26 Dec 2025; Revised 10 Feb 2026; Accepted 20 April 2026; Available online 30 April 2026
Digital Object Identifier (**DOI**): https://doi.org/10.35882/jeeemi.v8i2.1434

Table 4 summarizes the component-level ablation results of the proposed HRSA-Net architecture. The complete model achieves the best performance with an R^2 value of 0.834, MAE of 0.108, and RMSE of 0.172, indicating that the combination of Rough Set-based feature selection and the attention mechanism effectively improves BMD prediction accuracy. When the Rough Set module is removed, the model performance decreases to R^2 = 0.781, with MAE = 0.126 and RMSE = 0.194, demonstrating that feature reduction plays an important role in eliminating redundant impedance attributes. Similarly, removing the attention layer further reduces the performance to R^2 = 0.745, MAE = 0.140, and RMSE = 0.206, confirming that the attention mechanism contributes to capturing informative spectral features in high-dimensional EIS signals.

Table 4. Component-level ablation study results of the proposed HRSA-Net architecture.

Model Variant	Change Applied	R^2	MAE	RMSE
HRSA-Net (Proposed)	-	0.834	0.108	0.172
No Rough Set	Remove feature selector	0.781	0.126	0.194
No Attention	Remove attention layer	0.745	0.140	0.206
PCA instead of Rough Set	Swap Rough Set with PCA	0.768	0.133	0.198
Channel Attention	Use channel attention	0.821	0.115	0.179

Replacing Rough Set Theory with PCA results in slightly lower performance (R^2 = 0.768, MAE = 0.133, RMSE = 0.198), highlighting the advantage of rule-based dependency feature selection over linear dimensionality reduction methods [26]. In addition, the channel attention variant achieves R^2 = 0.821, MAE = 0.115, and RMSE = 0.179, which is slightly inferior to the proposed HRSA-Net, suggesting that the adopted attention design provides more effective feature weighting for impedance-based regression.

D. Learning Model Configuration

To ensure reproducibility of the proposed framework, detailed configurations of the learning models used in HRSA-Net are provided. Two regression backbones were evaluated in this study, namely an Artificial Neural Network (ANN) and a Transformer-based regression model [27][28]. Both models receive reduced impedance features generated by the Rough Set module as input. The ANN regressor consists of a fully connected feedforward architecture [27] composed of an input layer corresponding to the selected impedance features, followed by two hidden layers containing 128 and 64 neurons, respectively. Rectified Linear Unit (ReLU) activation functions [36] are employed in hidden layers to introduce nonlinearity, while a linear activation function is used in the output layer to produce continuous Bone Mineral Density (BMD) predictions. Dropout with a rate of 0.2 is applied to reduce overfitting during training. For enhanced regression capability, a Transformer-based regressor is also implemented [28].

Table 5. Architectural and training configuration of ANN and Transformer-Based regression models used in HRSA-Net

Parameter	ANN	Transformer
Hidden Layers	128-64	Enconder ×2
Activation	ReLU	GELU/ReLU
Attention Heads	-	4
Embedding Size	-	64
Optimizer	Adam	Adam
Learning Rate	0.001	0.001
Batch Size	32	32
Epoch	150	150

The model consists of two encoder layers with a model embedding dimension of 64 and four attention heads. Each encoder layer includes multi-head self-attention followed by position-wise feedforward networks. Layer normalization and residual connections are applied to stabilize training and improve convergence. The Transformer processes dependency-reduced impedance sequences to capture contextual relationships across frequency components. Both models are trained using the Adam optimizer [37] with an initial learning rate of 0.001 and a batch size of 32. Training is conducted for a maximum of 150 epochs with early stopping applied based on validation loss to prevent overfitting. The dataset is divided into training, validation, and testing subsets using a 70:15:15 ratio. A summary of the architectural and training configurations used for both regression backbones is presented in Table 5 to facilitate reproducibility and implementation clarity.

As summarized in Table 5, both regression models share identical optimization settings to ensure fair performance comparison. Specifically, both models are trained using the Adam optimizer, a learning rate of 0.001, a batch size of 32, and 150 training epochs. The ANN backbone employs a fully connected architecture with two hidden layers consisting of 128 and 64 neurons, using the ReLU activation function to perform nonlinear feature mapping. In contrast, the

Manuscript received 26 Dec 2025; Revised 10 Feb 2026; Accepted 20 April 2026; Available online 30 April 2026
Digital Object Identifier (**DOI**): https://doi.org/10.35882/jeeemi.v8i2.1434

Transformer-based regressor utilizes two encoder layers, four attention heads, and an embedding dimension of 64 to capture contextual dependencies among impedance features across frequency domains. Using identical training configurations allows the observed performance differences to be attributed primarily to architectural design rather than differences in optimization settings.

E. Model Training Strategy

The proposed HRSA-Net models were trained from scratch using the collected phantom-based Electrochemical Impedance Spectroscopy (EIS) dataset without employing pretrained weights or transfer learning strategies. This approach ensures that the regression models learn impedance–density relationships directly from experimentally acquired data. Prior to training, the dataset was randomly divided into training, validation, and testing subsets using a 70:15:15 ratio to ensure unbiased model evaluation. The training subset was used for parameter optimization, while the validation subset guided hyperparameter tuning and early stopping criteria. The independent testing subset was reserved exclusively for final performance evaluation.

During training, input features obtained from Rough Set-based reduction were normalized using z-score normalization to stabilize gradient updates and accelerate convergence [38]. Model parameters were optimized using the Adam optimizer [37], and early stopping was applied when validation loss failed to improve for 15 consecutive epochs, preventing overfitting [39]. All experiments were conducted using identical data partitions across evaluated model variants to ensure fair comparative analysis.

F. Loss Function Formulation

To evaluate regression performance under varying signal conditions, two loss functions were investigated in this study, namely Mean Squared Error (MSE) and Huber loss [40][41]. The selection of loss functions plays a critical role in determining model robustness, particularly when handling biomedical impedance measurements that may contain noise and measurement variability. The Mean Squared Error (MSE) loss is defined as the average squared difference between predicted and ground-truth Bone Mineral Density (BMD) values [40], as shown in Eq. (8).

$$MSE = \frac{1}{n}\sum_{i=1}^{n}(y_i - \hat{y}_i)^2 \quad (8)$$

where y_i represents the reference BMD value and $\hat{y}_i$ denotes the predicted output. MSE strongly penalizes large prediction errors due to the quadratic term, making it sensitive to outliers present in experimental biomedical datasets [40]. To improve robustness against abnormal measurement deviations, the Huber loss function is employed [41]. Huber loss combines the advantages of MSE and Mean Absolute Error (MAE) by applying quadratic penalization for small errors and linear penalization for large errors, as shown in Eq. (9).

$$L_\delta(e) = \begin{cases} \frac{1}{2}e^2, & |e| \le \delta \\ \delta\left(|e| - \frac{1}{2}\delta\right), & |e| > \delta \end{cases} \quad (9)$$

where e represents the prediction error and δ denotes a predefined transition threshold. In EIS-based measurements, impedance signals are susceptible to noise caused by electrode contact variation, environmental interference, and phantom measurement inconsistencies. Such variations may introduce outlier samples that disproportionately influence gradient updates when MSE loss is used. The Huber loss mitigates this issue by reducing sensitivity to large deviations while maintaining stable convergence for small prediction errors. Consequently, the use of Huber loss improves regression stability and contributes to the enhanced prediction accuracy observed in the experimental results.

G. Mathematical Modeling of EIT System

To provide a physical interpretation of impedance measurements used in this study, the Electrical Impedance Tomography (EIT) framework is briefly introduced. Electrical impedance reconstructs the spatial conductivity distribution inside an object by injecting electrical current through surface electrodes and measuring the resulting boundary voltages [42]. Under quasi-static conditions, where capacitive and inductive effects are negligible, the electrical impedance system can be modeled using a conductivity-based elliptic formulation derived from Maxwell's equations [42][43]. The electrical potential distribution $\phi(\mathrm{r})$ inside the domain $\Omega$is governed by the elliptic partial differential equation given in Eq. (10) [42][43].

$$\nabla . \left(\sigma(r)\nabla\emptyset(r)\right) = 0 \quad (10)$$

where $\sigma(\mathrm{r})$ represents the spatial electrical conductivity distribution and $\phi(\mathrm{r})$ denotes the electrical potential. The boundary condition applied on the electrode surface $\partial\Omega$ follows the complete electrode model (CEM) [44][49], as expressed in Eq. (11).

$$\emptyset + z_1\sigma\frac{\partial\emptyset}{\partial n} = V_1, \text{ on electrode } l \quad (11)$$

where z_l is the contact impedance of the l-th electrode, V_l is the measured electrode voltage, and $\partial\phi/\partial n$ denotes the normal derivative. The injected current satisfies the conservation law given in Eq. (12).

$$\int_{E_1}^{E_l}\sigma\frac{\partial\emptyset}{\partial n}dS = I_1 \quad (12)$$

where I_l represents the applied current on the electrode l. To solve the forward problem, the domain $\Omega$is discretized using the Finite Element Method (FEM) [42][45]. This discretization leads to a linearized system

Manuscript received 26 Dec 2025; Revised 10 Feb 2026; Accepted 20 April 2026; Available online 30 April 2026
Digital Object Identifier (**DOI**): https://doi.org/10.35882/jeeemi.v8i2.1434

relating the conductivity distribution and the boundary voltage measurements, as shown in Eq. (13).

$$V = J\sigma \quad (13)$$

where V is the boundary voltage vector, σ is the discretized conductivity vector, and J is the Jacobian (sensitivity) matrix. The inverse problem aims to estimate σ from the measured voltage data. Since this problem is ill-posed and nonlinear, regularized iterative reconstruction methods are employed to obtain a stable conductivity image [43][46]. In this study, the EIT formulation provides the physical foundation for interpreting impedance measurements obtained from the bone phantom model. Variations in reconstructed conductivity distributions correspond to changes in bone mineral composition, which are subsequently represented through Electrochemical Impedance Spectroscopy (EIS) features used as inputs to the proposed HRSA-Net learning framework. Therefore, the EIT model establishes the relationship between electrical conductivity behavior and Bone Mineral Density (BMD) estimation.

III. Result

A. Accuracy and Hyperparameter Performance

To further investigate the performance sensitivity of HRSA-Net framework, several variations in hyperparameter settings were evaluated while maintaining the same core architecture. The purpose of this evaluation is to examine how different design choices influence the accuracy of bone mineral density estimation. The evaluated configurations include variations in input representation, loss function, and regression backbone. Specifically, the experiments compare raw magnitude input with phase-augmented input, mean squared error loss with Huber loss, and artificial neural network regressors with Transformer-based regressors. The quantitative performance results of these configurations are summarized in Table 6.

As shown in Table 6, the original HRSA-Net configuration using an ANN backbone with raw magnitude input and MSE loss achieves a baseline performance of R^2 = 0.834, MAE = 0.108, and RMSE = 0.172. Replacing the MSE loss with the Huber loss slightly improves the performance to R^2 = 0.841, with reduced errors (MAE = 0.104, RMSE = 0.166), indicating better robustness to potential outliers in impedance measurements. When richer input features combining magnitude and phase information are introduced, the model achieves further improvement with R^2 = 0.844, MAE = 0.102, and RMSE = 0.162, suggesting that phase information contributes additional discriminative impedance characteristics. Finally, integrating the Transformer-based regressor with log-magnitude features and Huber loss yields the best overall performance, achieving R^2 = 0.855, MAE = 0.098, and RMSE = 0.158. These results demonstrate the synergistic effect of optimized input representation, robust loss functions, and advanced regression architectures in improving BMD prediction accuracy.

Table 6. Quantitative performance results of HRSA-Net under different hyperparameter configurations.

HRSA-Net Variant	Loss Function	Input Type	Back Bone	R^2	MAE	RMSE	MSE
Original (Ablation Setting)	MSE	Raw Magnitude	ANN	0.834	0.108	0.172	0.029
With Huber Loss	Huber	Raw Magnitude	ANN	0.841	0.104	0.166	0.028
With (Magnitude+Phase Input)	MSE	Magnitude+Phase	ANN	0.844	0.102	0.162	0.026
With Log-Magnitude Input	MSE	Log-Magnitude	ANN	0.843	0.103	0.163	0.027
With Transformer Regressor	MSE	Log-Magnitude	Transformer	0.846	0.101	0.161	0.026
Final Comparasion Version	Huber	Magnitude+Phase	Transformer	0.855	0.098	0.158	0.025

B. Performance Comparison Across Model Variants

To provide a broader assessment of the proposed framework, the regression performance of multiple learning model variants was quantitatively compared. This comparison aims to evaluate how different architectural combinations affect predictive accuracy. The comparative regression results across the evaluated model variants are presented in Table 7. Table 7 summarizes the quantitative regression performance of the evaluated learning model variants using R^2, MAE, RMSE, and MSE metrics. The baseline ANN model achieves an R^2 value of 0.672, MAE of

Manuscript received 26 Dec 2025; Revised 10 Feb 2026; Accepted 20 April 2026; Available online 30 April 2026
Digital Object Identifier (**DOI**): https://doi.org/10.35882/jeeemi.v8i2.1434

Table 7. Quantitative regression performance comparison across different HRSA-Net ablation variants.

Model	R^2	MAE	RMSE	MSE
Baseline ANN	0.672	0.168	0.238	0.056
RoughNet	0.745	0.139	0.205	0.042
AttnNet	0.781	0.126	0.194	0.037
HRSA-Net (Proposed)	0.834	0.108	0.172	0.029
RS + Channel Attention	0.821	0.115	0.179	0.032
PCA-AttnNet	0.768	0.133	0.198	0.039
RS + No Attention	0.745	0.140	0.206	0.042
RS + Attn + BiLSTM	0.840	0.105	0.167	0.027
RS + Attn + Transformer	0.846	0.101	0.161	0.026
RS + Attn + Transformer (Huber)	0.855	**0.098**	0.158	0.025

0.168, and RMSE of 0.238, serving as the reference performance without feature selection or attention mechanisms. Introducing Rough Set–based feature selection improves the performance to R^2 = 0.745, while the attention-based model (AttnNet) further increases the predictive capability to R^2 = 0.781, with reduced error values (MAE = 0.126, RMSE = 0.194). The proposed HRSA-Net configuration achieves a higher performance of R^2 = 0.834, demonstrating the advantage of combining rule-based feature selection with attention mechanisms for impedance-based regression tasks. Further architectural enhancements continue to improve prediction accuracy. For instance, integrating BiLSTM results in R^2 = 0.840, while incorporating a Transformer-based regressor increases the performance to R^2 = 0.846. The best overall performance is obtained by the HRSA-Net variant combining Rough Set, attention mechanisms, Transformer regression, and Huber loss, achieving R^2 = 0.855, MAE = 0.098, and RMSE = 0.158. This represents a substantial improvement over the baseline ANN model, confirming the effectiveness of combining feature reduction, attention-based feature weighting, and advanced regression architectures for accurate BMD prediction.

C. Configuration Summary of Learning Model Variants

To support the interpretation of the quantitative results presented in the previous sections, a structured overview of the architectural and training configurations corresponding to each evaluated learning model variant is provided. This overview is intended to clarify the key design components adopted in each model, including feature selection, attention mechanism, regression architecture, and input representation. This structured summary facilitates direct mapping between the observed performance outcomes and the specific architectural or training choices employed in each configuration. The detailed configuration information for all evaluated learning model variants is summarized in Table 8.

The configuration summary in Table 8 presents the architectural components of each evaluated learning model variant, including feature selection strategy, attention mechanism, regression model, and input representation. Several configurations introduce individual architectural components to enable systematic comparison across model designs. In addition to single-component variants, combined configurations integrate Rough Set feature selection with attention mechanisms and different regression backbones. This structured summary provides a clear

Table 8. Configuration summary of evaluated learning model variants used in this study.

Model	Feature Selector	Attention	Regressor	Input Type	Loss
Baseline ANN	-	-	ANN	Raw Magnitude	MSE
RoughNet	Rough Set	-	ANN	Raw Magnitude	MSE
AttnNet	-	Self-attention	ANN	Raw Magnitude	MSE
HRSA-Net (Ours)	Rough Set	Self-attention	ANN	Raw Magnitude	MSE
RS + Channel Attention	Rough Set	Channel Attention	ANN	Raw Magnitude	MSE
PCA-AttnNet	PCA	Self-attention	ANN	Raw Magnitude	MSE
RS + No Attention	Rough Set	-	ANN	Raw Magnitude	MSE

Manuscript received 26 Dec 2025; Revised 10 Feb 2026; Accepted 20 April 2026; Available online 30 April 2026
Digital Object Identifier (**DOI**): https://doi.org/10.35882/jeeemi.v8i2.1434

reference for relating each model variant to the quantitative performance differences reported in Tables 5 and 8.

D. Comparative Summary of Related EIS-Based Learning Studies

To contextualize the proposed HRSA-Net framework within existing research on EIS-based learning approaches, a comparative summary of representative studies is presented. This comparison highlights methodological characteristics reported in prior work. The comparative summary of related EIS-based learning studies is shown in Table 9. Table 9 presents a comparative overview of previously reported EIS-based learning approaches, including the input modality, learning task, and output parameter. The listed studies primarily focus on classification or categorical prediction tasks, such as glucose level detection, motion classification, or health state assessment, using various machine learning architectures. In contrast, the proposed HRSA-Net addresses continuous bone mineral density regression, which remains relatively underexplored in prior EIS-based learning studies. This comparison highlights the distinct positioning of the present work within the existing literature and provides context for evaluating the architectural and task-level differences between HRSA-Net and previously reported EIS-based approaches.

E. Visualization of Regression Results

To complement the quantitative evaluation results, visual comparisons between predicted and actual bone mineral density values are provided. These visualizations are intended to offer an intuitive representation of the prediction behavior of the evaluated models across the BMD range. The scatter plots depict the relationship between the predicted and actual bone mineral density values, enabling qualitative assessment of prediction accuracy and error distribution. Alignment of data points with the ideal regression line indicates stronger agreement between model

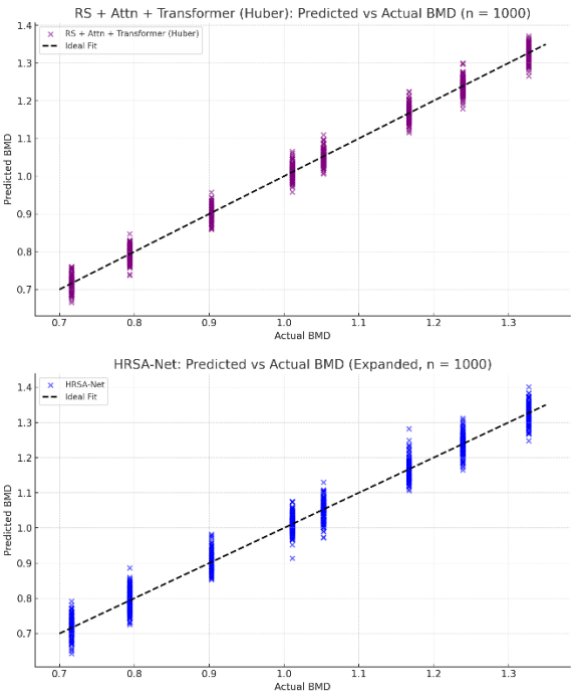

Fig. 2. Comparison of predicted and actual bone mineral density values for (a) HRSA-Net (R^2 = 0.834) and (b) RS with Attention and Transformer-Based regression model (R^2 = 0.846).

predictions and ground-truth values. The predicted versus actual regression results for the evaluated models are illustrated in Fig. 2, serving as a visual counterpart to the numerical performance metrics reported in the previous sections. Fig. 2 illustrates the visual comparison between predicted and actual bone mineral density values for the evaluated models. The plots present regression outcomes for (a) the original HRSA-Net configuration and (b) the RS + Attention + Transformer variant, enabling qualitative assessment of prediction accuracy and error distribution. As shown in Fig. 2, both models demonstrate a strong alignment

Table 9. Comparative overview of architectural designs in EIS-Based learning methods reported in the literature.

Reference	Input Type	Learning Model	Task Type	Output
[32]	EIS (Synthetic Bone)	Random Forest / ML	Regression	Bone Mineral Content
[34]	EIS (Soil)	LSTM	Regression	Nitrate Concentration
[40]	Sensor Signals	Robust OED (Gradient)	Optimization	Sensor Failure Prediction
[41]	Crack Signals	ResNet + CBAM	Regression	Crack Size Estimation
[50]	Bioimpedance	Equivalent Spectrum	Regression	Blood Glucose Level
[51]	EIS (Bio-signal)	Backpropagation (ANN)	Classification	Diabetes Mellitus Stage

Manuscript received 26 Dec 2025; Revised 10 Feb 2026; Accepted 20 April 2026; Available online 30 April 2026
Digital Object Identifier (**DOI**): https://doi.org/10.35882/jeeemi.v8i2.1434

between predicted and actual BMD values across the evaluated range. The Transformer-based variant exhibits a tighter clustering of prediction points around the ideal regression line, reflecting reduced prediction error and more consistent estimation behavior. These visual results complement the quantitative performance metrics reported earlier.

IV. Discussion

A. Overall Interpretation of the Quantitative Findings

The present results demonstrate that the proposed HRSA-Net framework is capable of learning a clinically meaningful mapping between frequency-dependent EIS measurements and continuous Bone Mineral Density (BMD) values. Among all evaluated configurations, the best-performing variant, which combines Rough Set-based feature reduction, attention-guided learning, a Transformer regressor, and Huber loss, achieved an $\boldsymbol{R^2}$of 0.855, an MAE of 0.098, an RMSE of 0.158, and an MSE of 0.025. This performance is substantially better than that of the baseline ANN model, which produced an $\boldsymbol{R^2}$of 0.672, an MAE of 0.168, an RMSE of 0.238, and an MSE of 0.056. In absolute terms, the final model improves $\boldsymbol{R^2}$by 0.183, while reducing MAE by 0.070 and RMSE by 0.080. These margins are not trivial; they indicate that the proposed framework does not merely fit the data more closely, but does so with a consistently lower prediction error across the BMD range. In the context of non-radiative BMD estimation, this is important because even moderate reductions in regression error may improve the practical reliability of screening-oriented systems derived from EIS measurements. Another important observation is that model improvement was incremental and coherent across architectural refinements rather than being caused by a single isolated modification. The original HRSA-Net configuration already achieved $R^2 = 0.834$, indicating that the combination of Rough Set reduction and self-attention was effective even before introducing a more advanced regressor. Performance then increased to $R^2 = 0.841$ when Huber loss was used, to $R^2 = 0.844$ when richer impedance information was introduced, and to $R^2 = 0.846$ when the Transformer backbone was adopted, before reaching the final $R^2 = 0.855$. This progressive pattern suggests that the reported gains are structurally meaningful and reflect the complementary roles of feature selection, adaptive weighting, robust optimization, and contextual sequence modeling. Such consistency strengthens the argument that HRSA-Net is not simply a better-tuned neural network, but rather a carefully constructed hybrid framework in which each component contributes to improved regression quality.

B. Effect Of Rough Set-Based Feature Reduction

The first contribution of this study lies in the integration of Rough Set Theory as an interpretable feature reduction mechanism for high-dimensional EIS data. The experimental evidence strongly supports the value of this component. The original impedance representation contained 96 attributes, which were reduced to 28 dependency-relevant features, corresponding to a dimensionality reduction of approximately 70.8%. This result is important for two reasons. First, it confirms that a large portion of the raw impedance space is likely redundant or only weakly informative for BMD regression. Second, it indicates that dependency-driven reduction can preserve predictive information while substantially simplifying the input space. In biomedical signal learning, where high-dimensional measurements often contain correlated or noisy variables, this type of reduction is especially valuable because it lowers the risk of overfitting and improves interpretability at the same time.

The ablation results further show that Rough Set reduction is not merely a preprocessing convenience, but a quantitatively relevant component of model performance. When the Rough Set module was removed, performance decreased from $R^2 = 0.834$to $R^2 = 0.781$, while MAE increased from 0.108 to 0.126 and RMSE increased from 0.172 to 0.194. Likewise, replacing Rough Set with PCA produced a lower $R^2$of 0.768, with higher MAE and RMSE values than the proposed configuration. This comparison is particularly meaningful because PCA is a well-known dimensionality reduction technique, yet it underperformed relative to Rough Set in this study. The most plausible interpretation is that linear variance-based compression is not sufficient for this problem, because EIS-derived BMD prediction depends not only on compact representation, but also on preserving dependency-relevant spectral attributes that remain informative for regression. Rough Set reduction, therefore, appears better aligned with the structure of impedance data, where the most useful features are not necessarily those explaining the largest global variance, but those most strongly associated with decision-relevant changes in mineral-related conductivity behavior.

B. Effect Of Rough Set-Based Feature Reduction

The second contribution concerns the use of attention-guided neural prediction to weight the relative importance of spectral features. This component is also strongly supported by the ablation study. Removing the attention mechanism reduced performance from $R^2 = 0.834$to $R^2 = 0.745$, while MAE increased from 0.108 to 0.140 and RMSE increased from 0.172 to 0.206. The magnitude of this drop is larger than the performance

Manuscript received 26 Dec 2025; Revised 10 Feb 2026; Accepted 20 April 2026; Available online 30 April 2026
Digital Object Identifier (**DOI**): https://doi.org/10.35882/jeeemi.v8i2.1434

reduction observed when Rough Set was removed, indicating that adaptive feature weighting is a major determinant of prediction quality in this task. This result is conceptually plausible because EIS signals are intrinsically frequency-dependent, and not all spectral regions are expected to contribute equally to the characterization of bone mineral composition. An attention mechanism is therefore appropriate not only from a machine learning perspective, but also from a signal interpretation perspective, since it allows the model to emphasize more informative impedance components while suppressing less relevant ones.

The comparison between self-attention and channel attention provides an additional layer of interpretation. The channel attention variant achieved $R^2 = 0.821$, which is better than several baseline variants but still lower than the proposed HRSA-Net. This suggests that not all weighting strategies are equally suitable for this regression task. The adopted self-attention formulation likely provides a more flexible mechanism for modeling dependencies among reduced impedance attributes, whereas channel attention may be more limited in capturing the broader contextual relationships needed for continuous BMD estimation. Similarly, the comparison across learning backbones shows that the use of a Transformer regressor further improved performance relative to the ANN-based HRSA-Net and the BiLSTM variant. The Transformer-based configuration reached $R^2 = 0.846$, while the BiLSTM variant reached $R^2 = 0.840$. The final Huber-based Transformer model then achieved $R^2 = 0.855$, confirming that the best results emerge when adaptive weighting is combined with a backbone that can model long-range inter-feature relationships more effectively.

The improvement obtained by the Huber loss also deserves interpretation. The shift from the original MSE-based HRSA-Net to the Huber-based configuration improved R^2 from 0.834 to 0.841 and reduced the error metrics consistently. This pattern supports the assumption that EIS measurements may contain outlier-like deviations caused by contact variation, environmental interference, or phantom acquisition inconsistencies. Under such conditions, a robust loss function is not just a technical alternative, but an important stabilization mechanism. Therefore, the overall evidence suggests that the predictive success of HRSA-Net arises from the interaction of three complementary principles: dependency-aware feature compression, adaptive spectral weighting, and robust contextual regression.

D. Non-Radiative Continuous BMD Estimation And Its Significance

A major conceptual contribution of this study is that it frames EIS not as a tool for coarse categorization, but as a basis for direct continuous BMD regression. This distinction is important. Several prior EIS-related studies summarized in the manuscript focused on moisture estimation, soil nitrate prediction, uncertainty estimation, battery health regression, tissue classification, glucose prediction, or other non-BMD tasks. Even when bone-related work is discussed in the introduction, much of the broader literature is described as classification-oriented or not explicitly designed for direct density regression. In contrast, the present framework is built around real-valued BMD prediction referenced to DXA measurements. This positions the work more closely to quantitative clinical assessment rather than simple state labeling.

This distinction also strengthens the practical relevance of the study. A regression framework is more useful than a categorical classifier when the goal is to support longitudinal monitoring, trend analysis, or early-stage screening, because continuous outputs can reflect gradual changes that may not yet cross diagnostic thresholds. For a radiation-free modality such as EIS, this is particularly meaningful. The present results, therefore, suggest that HRSA-Net may serve as a promising computational core for future portable or community-level systems intended to complement standard bone assessment workflows. At the same time, the results should be interpreted as supporting a complementary screening direction rather than a direct replacement for DXA. The current study demonstrates feasibility and strong predictive potential, but the clinical substitution claim would require considerably broader external validation and in vivo testing.

E. Comparison with Related EIS-Based Learning Studies

The comparison with related EIS-based learning studies should be interpreted carefully and conservatively. The manuscript correctly positions HRSA-Net as distinct from earlier EIS-learning work because many previous studies addressed different targets, different domains, or different task types. This means that the present study should not overclaim a direct metric-level superiority over all prior works, since dataset composition, biological context, signal acquisition conditions, and output definitions differ substantially. However, the present results do support three comparative advantages. First, the proposed framework addresses a relatively underexplored task, namely continuous BMD regression from EIS data. Second, it introduces an interpretable dependency-based reduction stage instead of relying solely on black-box end-to-end feature learning. Third, it demonstrates that combining Rough Set reduction with attention-guided regression yields consistent gains over simpler ANN, RoughNet, AttnNet,

Manuscript received 26 Dec 2025; Revised 10 Feb 2026; Accepted 20 April 2026; Available online 30 April 2026
Digital Object Identifier (**DOI**): https://doi.org/10.35882/jeeemi.v8i2.1434

PCA-AttnNet, and no-attention variants within the same experimental setting. These points make the contribution methodologically credible even without forcing unfair one-to-one metric comparisons with unrelated studies.

F. Limitations, Weaknesses, and Future Directions

Despite the encouraging results, several limitations should be explicitly acknowledged. First, the dataset is phantom-based rather than clinical in-vivo data. Although phantom experiments are useful for controlled proof-of-concept evaluation, they cannot fully capture the variability present in real patients, including differences in soft tissue composition, electrode placement, anatomical heterogeneity, hydration effects, and measurement noise arising from practical clinical acquisition. Second, the dataset contains 1000 samples drawn from eight phantom groups, with an imbalanced class-related distribution of 500 normal, 375 osteopenic, and 125 osteoporotic samples. While this is adequate for an initial regression study, it still limits the strength of generalization claims, especially for more severe bone loss categories. Third, all models were evaluated within a single experimental data source using a fixed partitioning strategy, which means that external validation, cross-device robustness, and cross-population reproducibility remain unresolved.

These limitations point directly to the next research steps. Future work should validate the framework on larger and more diverse datasets, including in-vivo or clinical cohorts, and should test whether the selected impedance features remain stable across acquisition setups and demographic subgroups. It would also be useful to examine calibration behavior, prediction uncertainty, and subgroup-specific errors across different BMD ranges, since a model intended for screening should be reliable not only on average, but also across clinically relevant strata. In addition, model compression and embedded implementation may be explored to support real-time portable deployment. Such developments would move the framework from methodological feasibility toward translational applicability in low-cost, non-radiative bone health monitoring.

G. Practical And Scientific Implications

Taken together, the findings indicate that accurate EIS-based BMD regression requires more than a generic neural model. The strongest performance emerged when the input space was first filtered using dependency-aware reduction, then weighted adaptively through attention, and finally modeled using a regression backbone capable of capturing richer inter-feature structure. Scientifically, this suggests that biomedical impedance learning benefits from architectures that combine interpretability, robustness, and contextual modeling rather than treating all spectral measurements as equally informative. Practically, the results support the possibility of developing safer and more accessible pre-screening tools for bone health assessment, especially in settings where DXA is costly, non-portable, or less feasible for repeated monitoring. Accordingly, the main implication of this study is not that EIS has already replaced radiological bone densitometry, but that it has become substantially more viable as a quantitative, non-radiative, and machine learning-assisted complementary pathway for BMD estimation.

V. Conclusion

This study presents HRSA-Net, a novel hybrid model designed to estimate bone mineral density (BMD) using Electrochemical Impedance Spectroscopy (EIS) data in a non-invasive, radiation-free manner. Our architecture effectively combines Rough Set theory and attention mechanisms to enhance signal interpretability and regression performance. Experimental results demonstrate that HRSA-Net achieves a regression accuracy of up to R^2 = 0.855 with an MAE of 0.098, outperforming conventional ANN-based approaches. Performance is further enhanced through the integration of Transformer-based regressors and Huber loss. Comparative analysis with prior studies highlights the capability of the proposed model for continuous BMD estimation, a domain that remains relatively underexplored. Future work will focus on validating the proposed framework using larger and more diverse datasets, as well as exploring real-time implementation and clinical translation of the system.

Acknowledgment

The authors would like to express their sincere gratitude to the Department of Biomedical Engineering, Faculty of Engineering, Universitas Dian Nuswantoro, Semarang, for the support and facilities provided throughout this research. The academic environment and technical resources contributed significantly to the completion of this study.

Funding

This research received no specific grant from any funding agency in the public, commercial, or not-for-profit sectors.

Data Availability

The datasets generated and analyzed during the current study are not publicly available due to institutional and ethical restrictions, but are available from the corresponding author upon reasonable request.

Manuscript received 26 Dec 2025; Revised 10 Feb 2026; Accepted 20 April 2026; Available online 30 April 2026
Digital Object Identifier (**DOI**): https://doi.org/10.35882/jeeemi.v8i2.1434

Author Contribution

Aripin contributed to the conceptualization and overall supervision of the study. Mauldy Nawa was responsible for model development, data analysis, and manuscript drafting. Eunike Laurensya and Zulhendra Adi assisted in data processing, experimental validation, and result analysis. Susilo contributed to methodological design and technical implementation. Sari Ayu assisted in data interpretation and manuscript review. All authors reviewed and approved the final manuscript and agreed to be accountable for all aspects of the work.

Declarations

Ethical Approval

This study was conducted in accordance with ethical standards and has received ethical clearance from the Health Research Ethics Committee of Poltekkes Kemenkes Semarang, Indonesia. All procedures were performed in compliance with relevant ethical guidelines, and informed consent was obtained from all participants prior to data acquisition.

Consent for Publication Participants.

Consent for publication was given by all participants

Competing Interests

The authors declare no competing interests.

References

[1] J. A. Kanis, N. C. Harvey, E. McCloskey, H. Johansson, and C. Oden, “European guidance for the diagnosis and management of osteoporosis,” *Osteoporos. Int.*, vol. 30, pp. 3–44, 2019. doi:10.1007/s00198-018-4704-5.

[2] NIH Consensus Development Panel, “Osteoporosis prevention, diagnosis, and therapy,” *JAMA*, vol. 285, no. 6, pp. 785–795, 2001. doi:10.1001/jama.285.6.785.

[3] J. A. Kanis, L. J. Melton III, C. Christiansen, C. C. Johnston, and N. Khaltaev, “The diagnosis of osteoporosis,” *J. Bone Miner. Res.*, vol. 9, no. 8, pp. 1137–1141, 1994. doi:10.1002/jbmr.5650090802.

[4] G. M. Blake and I. Fogelman, “The role of DXA bone density scans in the diagnosis and treatment of osteoporosis,” *Postgrad. Med. J.*, vol. 83, pp. 509–517, 2007. doi:10.1136/pgmj.2007.057505.

[5] E. M. Lewiecki, “DXA in clinical practice,” *Bone*, vol. 104, pp. 15–21, 2017. doi:10.1016/j.bone.2017.01.017.

[6] Armañac-Julián P, Kontaxis S, Rapalis A, Marozas V, Laguna P, Bailón R, Gil E and Lázaro J (2022) Reliability of pulse photoplethysmography sensors: Coverage using different setups and body locations. Front. Electron. 3:906324. doi: 10.3389/felec.2022.906324.

[7] Y. Moon, Z. Dong, S. K. Lee, et al., "Bioelectrical impedance analysis of bone mineral content based on dual-energy X-ray absorptiometry: evaluation of age-stratified optimized models," *Sci. Rep.*, vol. 15, p. 24658, 2025. DOI: 10.1038/s41598-025-08304-8.

[8] K. Ain, A. P. Putra, O. N. Rahma, D. Hikmawati, A. Rahmatillah, and C. A. C. Abdullah, "Electrical Impedance Spectroscopy as a Potential Tool for Detecting Bone Porosity," *Sensors and Actuators A: Physical*, vol. 370, p. 115252, 2024. DOI: 10.1016/j.sna.2024.115252.

[9] M. Aldobali, K. Pal, and H. Chhabra, "Noninvasive health monitoring using bioelectrical impedance analysis," in *Computational Intelligence in Healthcare Applications*, R. Agrawal, M.A. Ansari, R.S. Anand, S. Sneha, and R. Mehrotra, Eds. Academic Press, 2022, ch. 14, pp. 209–236. DOI: 10.1016/B978-0-323-99031-8.00008-9.

[10] N. Fukase *et al.*, "Wireless Measurements Using Electrical Impedance Spectroscopy to Monitor Fracture Healing," *Sensors*, vol. 22, no. 16, p. 6233, Aug. 2022. DOI: 10.3390/s22166233.

[11] Y. M. Liu, S. Q. Li, G. Q. Liu, Z. G. Lyu, and Z. W. Cui, "The Experimental Study of Bone Quality Assessment Based on Cole-Cole Parameter Characterization," in *The Proceedings of the 19th Annual Conference of China Electrotechnical Society (ACCES 2024)*, vol. 1409, Q. Yang, Z. Bie, and X. Yang, Eds. Singapore: Springer, 2025, pp. (nomor halaman jika ada). DOI: 10.1007/978-981-96-4787-3_65.

[12] T. K. Vashishth, V. Sharma, K. K. Sharma, B. Kumar, S. Chaudhary, and R. Panwar, "Enhancing biomedical signal processing with machine learning: A comprehensive review," in *Digital Transformation in Healthcare 5.0: Volume 1: IoT, AI and Digital Twin*, Berlin, Germany: De Gruyter, 2024, ch. 10, pp. 277–306. DOI: 10.1515/9783111327853.

[13] Z. Shao, J. Wu, Q. Deng, L. Cheng, X. Huang, W. Sun, W. Liang, and H. Li, "Development of a machine learning-based predictive model for osteoporosis risk and its application in clinical decision support," *Front. Med.*, vol. 12, p. 1680731, 2025. DOI: 10.3389/fmed.2025.1680731.

[14] R. Bagaria, S. Wadhwani, and A. K. Wadhwani, "Bone fractures detection using support vector

Manuscript received 26 Dec 2025; Revised 10 Feb 2026; Accepted 20 April 2026; Available online 30 April 2026
Digital Object Identifier (**DOI**): https://doi.org/10.35882/jeeemi.v8i2.1434

machine and error backpropagation neural network," *Optik*, vol. 247, p. 168021, 2021. DOI: 10.1016/j.ijleo.2021.168021.

[15] A. A. Ewees, M. E. Abd Elaziz, R. Arafa, and R. Ghoniem, "Improved Approach Based on Fuzzy Rough Set and Sine-Cosine Algorithm: A Case Study on Prediction of Osteoporosis," *IEEE Access*, vol. 8, pp. 203190–203202, 2020. DOI: 10.1109/ACCESS.2020.3036831.

[16] M. F. Dar and A. Ganivada, "Fuzzy rough set loss for deep learning-based precise medical image segmentation," *Comput. Med. Imaging Graph.*, vol. 128, p. 102716, Feb. 2026. DOI: 10.1016/j.compmedimag.2026.102716.

[17] Y. Sato, N. Yamamoto, N. Inagaki, Y. Iesaki, T. Asamoto, T. Suzuki, and S. Takahara, "Deep Learning for Bone Mineral Density and T-Score Prediction from Chest X-rays: A Multicenter Study," *Biomedicines*, vol. 10, no. 9, p. 2323, Sep. 2022. DOI: 10.3390/biomedicines10092323.

[18] Z. Lin, Z. Q. Lang, L. Guo, et al., "Deep learning-based electrical impedance spectroscopy analysis for malignant and potentially malignant oral disorder detection," *Sci. Rep.*, vol. 15, p. 19458, 2025. DOI: 10.1038/s41598-025-05116-8

[19] K. Umam, I. K. E. Purnama, R. F. Rachmadi, and S. A. Wulandari, "Detection of Mycobacterium Tuberculosis Using Real-time Detection Transformer," in *2024 International Seminar on Intelligent Technology and Its Applications (ISITIA)*, Mataram, Indonesia, 2024, pp. 633–638. DOI: 10.1109/ISITIA63062.2024.10667784

[20] S. A. Wulandari, I. K. E. Purnama, E. M. Yuniarno, and M. H. Purnomo, "Multicluster Kernel Intuitionistic Fuzzy C-Means and State Transition Algorithm: Framework for Low Light Segmentation Imaging of Tuberculosis Bacilli Base of Semisupervised Approach," in *2024 IEEE International Conference on Fuzzy Systems (FUZZ-IEEE)*, Yokohama, Japan, 2024, pp. 1–10. DOI: 10.1109/FUZZ-IEEE60900.2024.10612071

[21] S. A. Wulandari, I. K. E. Purnama, and M. H. Purnomo, "Auto Thresholding Sputum Color Image Segmentation For Tuberculosis Diagnosis Base On Intuitionistic Fuzzy," in *2022 International Conference on Computer Engineering, Network, and Intelligent Multimedia (CENIM)*, Surabaya, Indonesia, 2022, pp. 151–156. DOI: 10.1109/CENIM56801.2022.10037568.

[22] S. A. Wulandari, E. L. Agata, N. M. C. E, N. Alriski, M. T. Wafa'Ana, and A. Aripin, "Attention-Enhanced CNN-BiLSTM for Bone Mineral Density Estimation from Electrochemical Impedance Spectra," in *2025 International Seminar on Application for Technology of Information and Communication (iSemantic)*, Semarang, Indonesia, 2025, pp. 260–266. DOI: 10.1109/ISemantic67418.2025.11291862

[23] D. Nurdiyah, E. M. Yuniarno, S. A. Wulandari, Y. K. Surapto, and M. H. Purnomo, "Deep Semantic Feature Extraction to Overcome Overlapping Frequencies for Instrument Recognition in Indonesian Traditional Music Orchestras," *IEEE Access*, vol. 12, pp. 76936–76954, 2024. DOI: 10.1109/ACCESS.2024.3401699.

[24] Muljono, P. N. Andono, S. A. Wulandari, H. A. Azies, and M. Naufal, "Deep learning for audio signal-based tempo classification scenarios," *IAES Int. J. Artif. Intell.*, vol. 13, no. 2, pp. 1687–1701, Jun. 2024. DOI: 10.11591/ijai.v13.i2.pp1687-1701

[25] Muljono *et al.*, "Breaking Boundaries in Diagnosis: Non-Invasive Anemia Detection Empowered by AI," *IEEE Access*, vol. 12, pp. 9292–9307, 2024. DOI: 10.1109/ACCESS.2024.3353788.

[26] X. Yao, X. Zhang, E. Yang, and Y. Fan, "Variable precision -fuzzy rough sets and their applications in image processing and fuzzy decision trees," *Pattern Recognit.*, vol. 179, pt. C, p. 113796, Nov. 2026. DOI: 10.1016/j.patcog.2026.113796.

[27] P. Jain and T. Som, "Multigranular rough set model based on robust intuitionistic fuzzy covering with application to feature selection," *Int. J. Approx. Reason.*, vol. 156, pp. 16–37, May 2023. DOI: 10.1016/j.ijar.2023.02.004.

[28] D. Formica and E. Schena, "Smart Sensors for Healthcare and Medical Applications," *Sensors*, vol. 21, no. 2, p. 543, Jan. 2021. DOI: 10.3390/s21020543.

[29] M. M. Sibhai, A. Alkhateeb, and S. B. Ahmed, "MEDFORMER-UR: Uncertainty-Routed Transformer for Medical Image Classification," *arXiv preprint arXiv:2604.08868*, Apr. 2026. DOI: 10.48550/arXiv.2604.08868.

[30] M. K. Umair, R. Waheed, M. F. Abrar, et al., "Time series electrocardiography (ECG) data for early prediction of cardiac arrest," *Sci. Rep.*, vol. 16, p. 9761, 2026. DOI: 10.1038/s41598-026-35788-9.

[31] H. A. Tinoco *et al.*, "Bio-structural monitoring of bone mineral alterations through electromechanical impedance measurements of a Piezo-device joined to a tooth," *Biomed. Eng. Lett.*, vol. 10, no. 4, pp. 603–617, Sep. 2020. DOI: 10.1007/s13534-020-00170-9.

Manuscript received 26 Dec 2025; Revised 10 Feb 2026; Accepted 20 April 2026; Available online 30 April 2026
Digital Object Identifier (**DOI**): https://doi.org/10.35882/jeeemi.v8i2.1434

[32] A. Banerjee, Y. Tai, N. V. Myung, and J. Nam, "Non-destructive characterization of bone mineral content by machine learning-assisted electrochemical impedance spectroscopy," *Front. Bioeng. Biotechnol.*, vol. 10, p. 961108, Sep. 2022. DOI: 10.3389/fbioe.2022.961108.

[33] M. Han et al., "Deep learning guided electrochemical impedance spectroscopy," *ACS Sensors*, vol. 9, pp. 214–224, 2024. doi: 10.1021/acssensors.3c02039.

[34] X. Ma, L. Bifano, and G. Fischerauer, "Evaluation of Electrical Impedance Spectra by Long Short-Term Memory to Estimate Nitrate Concentrations in Soil," *Sensors*, vol. 23, no. 2, p. 2172, Feb. 2023. DOI: 10.3390/s23042172.

[35] N. V. Minh *et al.*, "Physics-encoded machine learning for performance and emission prediction of nickel ferrite nanocatalyst and hydrogen-enriched biodiesel in diesel engines," *RSC Adv.*, vol. 16, no. 12, pp. 10798-10821, Feb. 2026, doi: 10.1039/d5ra09336h.

[36] E. Oostwal, M. Straat, and M. Biehl, "Hidden unit specialization in layered neural networks: ReLU vs. sigmoidal activation," *Phys. A Stat. Mech. Appl.*, vol. 564, p. 125517, Feb. 2021. DOI: 10.1016/j.physa.2020.125517.

[37] A. Dixit, A. Mandal, S. Sanyal, and S. S. Ganguli, "A Genetic-Evolutionary ADAM (G-ADAM) optimizer for semisupervised convolutional neural network-based acoustic impedance inversion," in *SEG Technical Program Expanded Abstracts 2021*, 2021, pp. 2208–2212. DOI: 10.1190/segam2021-3594593.1.

[38] X. Ji, W. Duan, J. Peng, and S. Yao, "Fuzzy rough set attribute reduction based on decision ball model," *Int. J. Approx. Reason.*, vol. 179, p. 109364, Apr. 2025. DOI: 10.1016/j.ijar.2025.109364.

[39] V. Diukarev and Y. Starukhin, "Proposed Methods for Preventing Overfitting in Machine Learning and Deep Learning," *Asian J. Res. Comput. Sci.*, vol. 17, no. 10, pp. 85–94, Oct. 2024. DOI: 10.9734/ajrcos/2024/v17i10511

[40] R. White *et al.*, "Robust Optimal Experimental Design Accounting for Sensor Failure," *arXiv preprint arXiv:2604.14497*, Apr. 2026. DOI: 10.48550/arXiv.2604.14497.

[41] L. Q. Trung, N. Kasai, M. Le, and K. Sekino, "Predicting actual crack size through crack signal obtained by advanced Flexible Eddy Current Sensor using ResNet integrated with CBAM and Huber loss function," *NDT & E Int.*, vol. 149, p. 103249, Oct. 2024. DOI: 10.1016/j.ndteint.2024.103249.

[42] J. A. Ribeiro and P. A. S. Jorge, "Applications of electrochemical impedance spectroscopy in disease diagnosis—A review," *Sensors Actuators Rep.*, vol. 8, p. 100205, Dec. 2024. DOI: 10.1016/j.snr.2024.100205.

[43] L.-F. Mao, S. K. Li, P. Cheng, and L. J. Zhang, "Addressing challenges inverse problem with convolutional neural networks and regulation techniques: Applications in extraction of physical parameters of semiconductors devices," *Int. J. Electr. Power Energy Syst.*, vol. 161, p. 110172, Oct. 2024. DOI: 10.1016/j.ijepes.2024.110172.

[44] J. Dardé, N. Nasr, and L. Weynans, "Immersed boundary method for the complete electrode model in electrical impedance tomography," *J. Comput. Phys.*, vol. 487, p. 112150, Aug. 2023. DOI: 10.1016/j.jcp.2023.112150.

[45] R. E. Meethal, A. Kodakkal, M. Khalil, *et al.*, "Finite element method-enhanced neural network for forward and inverse problems," *Adv. Model. and Simul. in Eng. Sci.*, vol. 10, no. 6, 2023. DOI: 10.1186/s40323-023-00243-1.

[46] R. Alaifari, "Ill-Posed Problems: From Linear to Nonlinear and Beyond," in *Harmonic and Applied Analysis*, F. De Mari and E. De Vito, Eds. Cham, Switzerland: Birkhäuser, 2021, pp. 101–142. DOI: 10.1007/978-3-030-86664-8_3

[47] Bhardwaj P, Rai DV, Garg ML, Mohanty BP. Potential of electrical impedance spectroscopy to differentiate between healthy and osteopenic bone. Clin Biomech (Bristol). 2018 Aug;57:81-88. doi: 10.1016/j.clinbiomech.2018.05.014. Epub 2018 May 26. PMID: 29960118.

[48] C. Liebich, J. N. Bartsch, I. Schubert, M.-L. von Bruehl, and C. Sander, "Electrical Impedance Spectroscopy Improves Skin Cancer Detection and Reduces the Number of Biopsies," *Dermato*, vol. 2, no. 2, pp. 21–29, 2022. DOI: 10.3390/dermato2020004.

[49] A. Crowell, J.S. Yakisich, T.N.G. Adams, "Electrical Impedance Spectroscopy to Discriminate Between Normal and Cancerous Mammalian Cells," *Biosensors (Basel)*, vol. 11, no. 10, p. 401, Oct. 2021, doi:10.3390/bios11100401.

[50] Q. Gong *et al.*, "Non-Invasive and Accurate Blood Glucose Detection Based on an Equivalent Bioimpedance Spectrum," *Appl. Sci.*, vol. 15, no. 3, p. 1266, Jan. 2025. DOI: 10.3390/app15031266.

[51] M. Faisal *et al.*, "Development of Electrical Impedance Spectroscopy (EIS) Technique to Classify Diabetes Mellitus Disease Using Machine Learning with Backpropagation Method," *Trends Sci.*, vol. 22, no. 9, p. 10309,

Manuscript received 26 Dec 2025; Revised 10 Feb 2026; Accepted 20 April 2026; Available online 30 April 2026
Digital Object Identifier (**DOI**): https://doi.org/10.35882/jeeemi.v8i2.1434

2025. DOI: 10.48048/tis.2025.10309.

[52] I. Amira *et al.*, "The Degradation Test of IBS (Injectable Bone Substitutes) Paste Scaffold Using EIS (Electrical Impedance Spectroscopy) Methods," *Jurnal Teknologi*, vol. 88, no. 1, Jan. 2026. DOI: 10.11113/jurnalteknologi.v88.23560.

[53] J. Chen *et al.*, "Machine learning-directed electrical impedance tomography to predict metabolically vulnerable plaques," *Bioeng. Transl. Med.*, vol. 9, no. 1, p. e10616, Oct. 2023. DOI: 10.1002/btm2.10616.

Author Biography

Aripin received a doctoral degree in Informatics Engineering (Computer Science Education). Since August 2001, he has been with Universitas Dian Nuswantoro, Semarang, Indonesia, where he is currently a faculty member in the field of informatics and computer science education. He has been actively involved in teaching, academic development, and higher education activities for more than two decades. His academic interests include informatics engineering, computer science education, and the development of educational technologies. Through his long-term involvement in academia, he has contributed to curriculum development, student supervision, and research activities related to information technology and education. He is also engaged in institutional academic and research initiatives at Universitas Dian Nuswantoro.

Mauldy Nawa Ayu Wulandari is an undergraduate student in the Biomedical Engineering Study Program, Faculty of Engineering, Universitas Dian Nuswantoro, Semarang, Indonesia. Her research interests include medical instrumentation as well as medical data and image processing. She has research experience through the MBKM Research Program at the Institute of Medical Education and Research Indonesia (IMERI), Faculty of Medicine, Universitas Indonesia, and has served as a Teaching Assistant for the Digital Image Instrumentation course. In addition, she has been actively involved in the Student Creativity Program (PKM) and was a participant in the 37th National Student Scientific Week (PIMNAS). She is proficient in C++, Python, and MATLAB, and has experience in research and fieldwork activities.

Eunike Laurensya Agata is an undergraduate student in the Biomedical Engineering Study Program, Faculty of Engineering, Universitas Dian Nuswantoro, Semarang, Indonesia. Her academic interests include medical instrumentation, biomedical signal and image processing, and e-health technology. She has participated in various academic trainings and workshops related to biomedical engineering, which have strengthened her understanding of healthcare technology development and its practical applications. In addition to her academic activities, she has organizational experience as a Secretary of the Faculty of Engineering Student Representative Council, where she developed skills in administration, communication, teamwork, and coordination. She is proficient in C++ and Python, and is interested in applying programming skills to support biomedical system development. Her main interests include biomedical technology innovation, digital health solutions, medical device development, and fieldwork-based research that contributes to improving healthcare services.

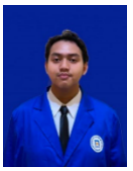

Zulhendra Adi Kusuma is an undergraduate student in the Biomedical Engineering Study Program, Faculty of Engineering, Universitas Dian Nuswantoro, Semarang, Indonesia. His research interests include medical instrumentation, applied biomedical technology, embedded systems, and biomedical device development. He has participated in various academic trainings and workshops related to engineering and technology, which have supported his understanding of both theoretical and practical aspects of biomedical system design. He is proficient in C++, VHDL, PCB design, and Microsoft Office, and is interested in applying these skills to the development of functional and efficient biomedical devices. His academic focus includes hardware-based medical technology, electronic circuit design, and instrumentation systems for healthcare applications. He also has a strong interest in research activities, prototype development, and collaborative projects that contribute to innovation in biomedical engineering.

Susilo is a lecturer in the Biomedical Engineering Department at Universitas Dian Nuswantoro, Semarang, Indonesia. He obtained his doctoral degree from the Faculty of Medicine, Universitas Diponegoro, after defending his dissertation entitled “Bone Imaging Using MATLAB-Based Software in Digital Radiography for the Diagnosis of Bone

Manuscript received 26 Dec 2025; Revised 10 Feb 2026; Accepted 20 April 2026; Available online 30 April 2026
Digital Object Identifier (**DOI**): https://doi.org/10.35882/jeeemi.v8i2.1434

Metastasis." His research focuses on the development of digital radiography systems, medical image processing, and MATLAB-based software to support diagnostic imaging analysis. His work is particularly related to the detection and evaluation of bone metastasis using digital radiographic images. The outcomes of his research have potential applications in both conventional radiography and Computed Radiography (CR) healthcare services. In addition to his research activities, he is involved in academic teaching, student supervision, and the development of biomedical engineering education, especially in areas related to medical imaging technology, radiological instrumentation, and healthcare-supporting software systems.

Sari Ayu Wulandari (Student Member, IEEE) obtained her master's degree in Electrical Engineering from Gadjah Mada University in 2011. Since 2021, she has been pursuing a doctoral degree at Institut Teknologi Sepuluh Nopember, Surabaya, Indonesia. She is currently a lecturer in the Biomedical Engineering Department at Universitas Dian Nuswantoro, Semarang, Indonesia, and a member of the CEMTI Laboratory, the Center for Medical Technology Innovation. Her research interests are in the field of biomedical engineering, particularly biomedical signal processing, medical image processing, artificial intelligence, and deep learning systems. Her current research focuses on the development of intelligent biomedical imaging methods for healthcare applications, including computer-aided diagnosis, medical image enhancement, segmentation, and classification. She is also actively involved in research and development activities related to medical instrumentation, digital health technology, and AI-based biomedical systems.

Manuscript received 26 Dec 2025; Revised 10 Feb 2026; Accepted 20 April 2026; Available online 30 April 2026
Digital Object Identifier (**DOI**): https://doi.org/10.35882/jeeemi.v8i2.1434